Spinon Fermi Surface in a Cluster Mott Insulator Model on a Triangular Lattice and Possible Application to 1T-TaS_2

Wen-Yu He,[1] Xiao Yan Xu,[1,*] Gang Chen,[2,3] K. T. Law,[1,‡] and Patrick A. Lee[4,†]
[1]*Department of Physics, Hong Kong University of Science and Technology, Clear Water Bay, Hong Kong, China*
[2]*State Key Laboratory of Surface Physics, Department of Physics,Center for Field Theory & Particle Physics, Fudan University, Shanghai 200433, China*
[3]*Collaborative Innovation Center of Advanced Microstructures, Nanjing 210093, China*
[4]*Department of Physics, Massachusetts Institute of Technology, Cambridge, Massachusetts 02139, USA*

(Received 12 March 2018; revised manuscript received 12 May 2018; published 24 July 2018)

1T-TaS_2 is a cluster Mott insulator on the triangular lattice with 13 Ta atoms forming a star of David cluster as the unit cell. We derive a two-dimensional XXZ spin-1/2 model with a four-spin ring exchange term to describe the effective low energy physics of a monolayer 1T-TaS_2, where the effective spin-1/2 degrees of freedom arises from the Kramers degenerate spin-orbital states on each star of David. A large scale density matrix renormalization group simulation is further performed on this effective model and we find a gapless spin liquid phase with a spinon Fermi surface at a moderate to large strength region of the four-spin ring exchange term. All peaks in the static spin structure factor are found to be located on the "$2k_F$" surface of a half-filled spinon on the triangular lattice. Experiments to detect the spinon Fermi surface phase in 1T-TaS_2 are discussed.

DOI: 10.1103/PhysRevLett.121.046401

Quantum spin liquid (QSL) was first proposed by Anderson in 1973 [1] and it has inspired a great deal of study of this state in frustrated magnetic systems. However, because of the lack of an obvious order parameter and symmetry breaking, QSL is very difficult to realize and characterize in experiments. During the last forty years people have only found a few QSL candidates [2–13], but still with many controversies in the details. The ongoing efforts are either in the direction to explore new QSL candidate materials [14,15], or push our theoretical and numerical understanding further.

It is well known that the geometric frustration on kagome, pyrochlore, and triangular lattices, or spin anisotropy such as the Kitaev type interaction on a honeycomb lattice [16], play an important role to stabilize a QSL phase [17]. On a kagome lattice, the isotropic nearest-neighbor antiferromagnetic Heisenberg interaction is probably enough to result in a QSL phase based on the density matrix renormalization group (DMRG) [18–21] or variational Monte Carlo (VMC) [22] calculations, while on a triangular lattice, this is not the case. The ground state of the Heisenberg model on the triangular lattice is the 120° AFM state [23–25]. Thus to stabilize QSLs, more frustration, such as next-neighbor frustrations [26–30], anisotropic [31], or high order exchange interaction is needed. The ring exchange terms become important for systems close to the insulating side of the Mott transition and it is suggested that the organics belongs with this case [32,33]. Exact diagonalization and variational study of the triangular lattice spin model with ring exchanges find a gapless QSL ground state with a spinon Fermi surface [32]. Later, DMRG simulation on two and four spin ladders and Gutzwiller variational wave functions calculation also find a similar QSL phase [34,35].

1T-TaS_2 was proposed to be a QSL candidate by two of us [10]. It has quasi-2D structure and each layer is made up of a triangular lattice with Ta atoms. It is recognized that 13-site clusters are formed with a very narrow band near the Fermi surface due to spin-orbit coupling (SOC) [36,37]. A weak residual repulsion interaction is enough to open a Mott gap. Charge fluctuations induce high order exchange processes for the local moments if the system is close to the Mott transition (a weak Mott insulator). There are good reasons to expect this to be the case for 1T-TaS_2 because it is the only insulator among all the CDW compounds and a related material 1T-$TaSe_2$ is metallic. This motivates us to derive an effective spin model that includes the effect of SOC and ring exchange. The geometric frustration and high order exchange interaction and spin anisotropy are new ingredients for the possible QSL physics in 1T-TaS_2. We use DMRG to explore the ground state properties of this effective spin model.

Effective spin model of 1T-TaS_2—In 1T-TaS_2, the Ta atoms form a planar triangular lattice sandwiched by S atoms in an octahedral coordination. The Ta layer and S layers have the ABC type stacking, which restores the global inversion symmetry for the crystal structure. As the temperature is lowered, 1T-TaS_2 undergoes a series of charge-density wave phase (CDW) transition and eventually entering the commensurate CDW phase around 180 K. This is the Mott insulating state [38] where the lattice is

deformed into a superlattice with the unit cell of a star of David, formed by 13 Ta clustered atoms seen from Fig. S1 (b) of the Supplemental Material [39]. In the $\sqrt{13}\times\sqrt{13}$ star of David unit cell, the outer twelve Ta atoms have displacement toward the centered Ta atom, which strengthens the interatomic bonds inside the star of David and weakens others. As the early first principles bulk band structure calculation for $1T$-TaS_2 indicates that the Ta $5d$ orbitals are dominant in the conduction and valence bands [37,44–47], the atomic SOC from $d_{x^2-y^2}$ and d_{xy} orbitals is expected to modify the reconstructed band structure in the commensurate CDW phase. Importantly, the joint effect of lattice deformation and atomic SOC gives rise to the well isolated narrow band at the Fermi level, as is shown in Fig. S1(a) of the Supplemental Material [39]. As a result, in the presence of weak repulsive interaction, the $1T$-TaS_2 is susceptible to the Mott-Hubbard transition and turns out to be a Mott insulator.

In order to describe the Mott state in the $1T$-TaS_2, we consider a single star of David unit cell as a supersite, which is described by the intracluster tight-binding Hamiltonian. Through numerical diagonalization, the Wannier orbitals localized inside the star of David with corresponding eigenenergies can be obtained in terms of the linear combination of atomic orbitals from the 13 Ta atoms. At the energy of the narrow band, it is found that the Wannier orbitals $\Psi_\alpha^\uparrow$ and $\Psi_\beta^\downarrow$ form the Kramers doublet while the Wannier orbitals $\Psi_\alpha^\downarrow$ and $\Psi_\beta^\uparrow$ are lifted in the energy due to the atomic SOC. Here the expressions for the two Wannier orbitals can be found in the Supplemental Material [39]. Taking the two Wannier orbitals as the basis, we can construct a two-orbital Hubbard model with both interorbital and intraorbital interactions for $1T$-TaS_2 [39]. Since each star of David unit cell occupied with the single state $\Psi_\alpha^\uparrow$ or $\Psi_\beta^\downarrow$ would have the lowest energy, all other occupation states can be perturbatively dealt with through the Schrieffer-Wolff transformation. As a result, the effective XXZ spin model with the anisotropy modified ring exchange terms can be obtained as

$$\begin{aligned}\tilde{\mathcal{H}}_{\mathrm{eff}} = J\sum_{\langle i,j\rangle}[S_i^xS_j^x+S_i^yS_j^y+(1+\gamma)S_i^zS_j^z]+K\sum_{\langle i,j,k,l\rangle}\{&[S_i^xS_j^x+S_i^yS_j^y+(1+\gamma)S_i^zS_j^z][S_k^xS_l^x+S_k^yS_l^y+(1+\gamma)S_k^zS_l^z]\\ &+[S_j^xS_k^x+S_j^yS_k^y+(1+\gamma)S_j^zS_k^z][S_i^xS_l^x+S_i^yS_l^y+(1+\gamma)S_i^zS_l^z]-(\boldsymbol{S}_i\cdot\boldsymbol{S}_k)(\boldsymbol{S}_j\cdot\boldsymbol{S}_l)\}.\end{aligned} \tag{1}$$

In the effective spin model, the J term is a XXZ type nearest-neighbor interaction, where γ denotes spin anisotropy, which arises as the ratio between the interorbital and intraorbital interaction deviates from 1 [39]. Because of the atomic SOC, the effective spin model does not have the SU(2) spin rotational symmetry but preserves the U(1) rotation around the z direction. Equation (1) is of general interest as an effective spin Hamiltonian including SOC. Therefore, given the large SOC in $1T$-TaS_2, the smallness of γ was not obvious *a priori* and required a demonstration. However, in practice it turns out that for $1T$-TaS_2 when the interorbital and intraorbital interactions are in the same order, the anisotropy γ remains smaller than 0.1 [39]. In the large limit of atomic SOC, the anisotropy γ will be further suppressed [39]. In the rest of the Letter we will mostly treat the case $\gamma = 0$. The K term is the four spin ring exchange term and is modified by the spin anisotropy. In general, the strength of K/J depends on the ratio between the effective in-plane hopping and interaction. In the weak Mott insulating regime, the effective hopping and interaction are at the same scale, which is verified in several first principle calculations of $1T$-TaS_2 [46,47], and then the strength of K/J is of order 1. The details on the derivation of the effective spin model and a comparing of parameters definition with earlier studied ring exchange model [32,34,35] can be found in the Supplemental Material [39].

For the spin model in Eq. (1), there are some well-known limits. (i) the $K/J = 0$, $\gamma = 0$ case. In this case, we have a pure Heisenberg model on the triangular lattice and the ground state is the famous 120° AFM state [23–25]. (ii) the $K/J = 0, \gamma \to \infty$ case. When $\gamma = \infty$, we have a pure Ising model on the triangular lattice. Because of the geometry frustration, the Ising spin does not order at zero temperature. As this paramagnetic state is highly degenerate, small perturbation may drive it to an ordered state via the order by disorder [48]. (iii) the $K/J = \infty$, $\gamma = 0$ case. In this case, we only have isotropic four-spin exchange terms. The ground state in the classical limit has been discussed in Ref. [49]. As in real materials, K is usually in the same order of J or smaller, this case is less relevant.

Results.—For general values of K/J and γ, the ground states are not known. To identify all possible ground states over a wide range of parameter space, we use DMRG to solve the effective spin model (1). The matrix product state (MPS) representation is used in our DMRG simulation. Because of the $U(1)$ spin rotational symmetry, the model has a total S^z conservation, and all results are obtained in the $S^z_{\mathrm{tot}} = 0$ sector [50]. We use the cylindrical geometry with open boundary condition in the x direction (see Fig. S4 of the Supplemental Material [39]). We use a bond dimension up to $m = 5120$ and all results are obtained with a truncation error in or less than the order of 10^{-5}.

To detect possible orders, we measure the spin-spin correlation $\langle \mathbf{S}_i \cdot \mathbf{S}_{i'}\rangle$, the dimer-dimer correlation $\langle D_b(i) D_b(i')\rangle - \langle D_b\rangle^2$ where $D_b(i) = \mathbf{S}_i \cdot \mathbf{S}_{i+\delta}$ (where $b = x, y, xy$ denotes $\delta = \hat{x}$, $\hat{y}$, or, $\hat{x}+\hat{y}$), and the chirality-chirality

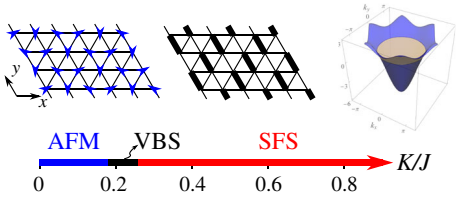

FIG. 1. Phase diagram for the isotropic case ($\gamma = 0$), while for the small anisotropy case related to real materials $1T$-TaS_2 the phase diagram is similar. It is mainly obtained from six wide systems and confirmed in eight wide systems.

correlation $\langle X_{\triangle} X_{\triangle'} \rangle$ where $X_{\triangle} = \mathbf{S}_i \cdot (\mathbf{S}_j \times \mathbf{S}_k)$ (with $i, j, k \in \triangle$). The phase diagram in Fig. 1 shows the results that we obtain mainly from six wide systems ($L_y = 6$) and confirm in eight wide systems ($L_y = 8$). Our work extends previous results done on four wide systems [34,35]. The details of finite size scaling to obtain the phase diagram can be found in the Supplemental Material [39]. It turns out the small anisotropy ($\gamma \lesssim 0.1$) only shifts the phase transition point slightly; thus we mainly focus on the isotropic case ($\gamma = 0$). At small K/J, the ground state is the 120° AFM state. In the intermediate value of K/J, a staggered valence bond solid (VBS) phase emerges. When $K/J > 0.3$, we enter a QSL state with a spinon Fermi surface (SFS). This state was called a spin Bose metal in some earlier literature [34,35].

We here focus on the SFS phase. In the SFS phase, all structure factors, including the spin, dimer, and chirality, shows no features of ordering. Thus we can rule out all spin, dimer, and chirality orders in this phase. Second, the real space correlations of spin-spin and dimer-dimer show long-range correlations and generally can be well fitted with power laws, as shown in Fig 2. The long range correlation is consistent with a gapless phase rather than a gapped one. In addition to a global power law decay in all these correlation functions, there are modulations and sign changes superposed over them. In the following, we will see the modulations in the spin correlator are actually the consequence of "$2k_F$" singularity due to the existence of a spinon Fermi surface. The modulation of the dimer correlator is discussed further in the Supplemental Material [39]. Thus the scatter of the data in Fig. 2 is due to these modulations and not due to numerical noise. As expected for a six-spin correlator, the chirality-chirality correlator shows much more rapid decay and can be fitted either with a large power law or an exponential. In addition, it exhibits sign changes. Thus we cannot interpret the chirality correlator in terms of the gauge flux correlator which is expected to have a power law decay with no sign changes in the asymptotic long distance limit. Apparently the system size is too small to reach that limit.

Another evidence for a gapless spin liquid comes from the finite static spin susceptibility. We calculate static spin susceptibility by applying small magnetic filed along the z direction. We find that the magnetic moment density and

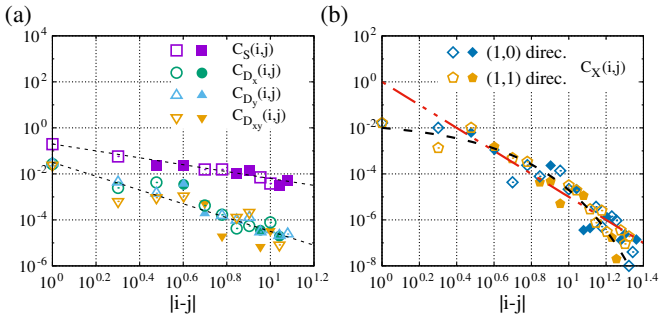

FIG. 2. (a) Real space decay of the spin-spin and dimer-dimer correlation, along the (1,0) direction. The absolute values are plotted, with open symbols and filled symbols denoting that the original values are negative or positive, respectively. The parameters are $L_x = 24$, $L_y = 6$, $K/J = 0.6$, $\gamma = 0$. In the log-log plot, all the correlation decays can be fitted with power law. Two power law lines are plotted to guide the eyes, the top black dashed line is $|i-j|^{-1.5}$, the bottom black dashed line is $|i-j|^{-3}$. (b) Real space decay of the chirality-chirality correlation along the (1,0) and (1,1) directions with the same parameters. It can be well fitted by either a high power law $|i-j|^{-5}$ (red dashed line) or an exponential decay $10^{-0.3|i-j|}$ (black dashed line).

magnetic fields obey a linear behavior and we get a finite static spin susceptibility ($\chi \approx 0.22$ for $K/J = 0.8$, where J and $g\mu_B$ are set to 1). Considering a half-filled free spinon band theory (static spin susceptibility is predicted to be $(g\mu_B)^2 N(0)/4$, where density of states at Fermi surface is about $N(0) \approx (1/1.65\pi t)$ with t the spinon hopping parameter), we can estimate the spinon hopping t to be $\sim 0.22J$. This estimate is not precise because we expect Fermi liquid corrections to the free spinon expression for the susceptibility. The important point is that the finite spin susceptibility is consistent with a gapless spin liquid with a spinon Fermi surface.

In order to confirm the SFS state, we look for $2k_F$ peaks in the spin structure factor $S(\mathbf{k})$. To simplify the discussion, we write $\mathbf{k}$ in the basis of reciprocal lattice primitive vectors $\mathbf{b}_1$ and $\mathbf{b}_2$, namely, $\mathbf{k} = k_1\mathbf{b}_1 + k_2\mathbf{b}_2$. We analyze the spin structure factor $S(\mathbf{k})$ for each fixed k_2 line, and pick out all peaks, as is shown in Figs. 3(a) to 3(d). The positions of all those peaks are plotted in Fig. 3(e). Here results of both $L_y = 6$ and $L_y = 8$ wide systems are plotted together. All the points are located on the $2k_F$ surface of a half-filled spinon on the triangular lattice, within finite size resolution. This strong signature of the existence of the spinon Fermi surface is a definitive evidence for the SFS phase.

We point out that there is an unexpected feature of the spin structure factor, namely there is no peak at the $2k_F$ position along the $\mathbf{b}_1$ line. This is seen in Fig. 3(d) ($k_2 = 0$ curve) and agrees with earlier results on four wide systems [35]. An interesting possibility is that a gap is open along the Γ (0,0) to M $(\frac{1}{2}, 0)$ directions due to spinon pairing. The Amperean scenario proposed by Lee *et al.* [51] will create a set of gaps separated by spinon Fermi arcs. In this case

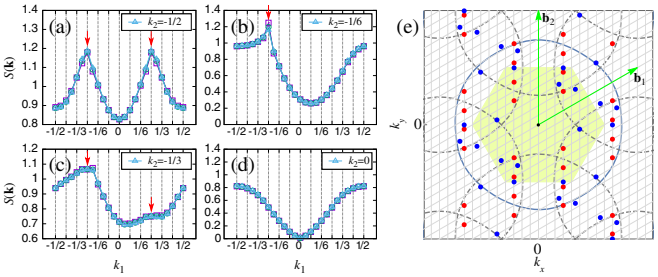

FIG. 3. Spin structure factor for different k_2 lines. Square, circle, and triangular points are the results of $m = 1280$, 2560, and 5120, respectively, where the overlap of those three points indicates the well convergence of the spin structure factor. Here the parameter is $L_y = 6$, $L_x = 24$, $K/J = 0.8$, $\gamma = 0$, in SFS phase. The red arrows denote peaks. The positions of peaks are $(\pm\frac{1}{4}, -\frac{1}{2})$ in (a); $(-\frac{1}{4}, -\frac{1}{6})$ in (b); $(\pm\frac{1}{4}, -\frac{1}{3})$ in (c). For $k_2 > 0$, there are also peaks, the positions are inversion images of the above points. (e) Positions of peaks in spin structure factor with parameter $K/J = 0.8$, $\gamma = 0$, in SFS phase. The red points are from the $L_y = 6$, $L_x = 24$ system, and the blue points are from the $L_y = 8$, $L_x = 24$ system. The solid blue line is the $2k_F$ surface line, with k_F is the Fermi vector of half-filled free spinon on the triangular lattice. Dashed gray lines are from translation of $2k_F$ along $\mathbf{b}_1$, $\mathbf{b}_2$ and $\mathbf{b}_1 - \mathbf{b}_2$. Grid size of gray mesh corresponds to $\frac{1}{12}$ of the reciprocal lattice vector. Light yellow shadowed region denotes the first Brillouin zone.

the spin liquid will belong to the class of Z2 QSL with spinon Fermi surface. Further discussion of this possibility and its relation to the structure of the dimer correlator can be found in the Supplemental Material [39].

The partially filled spinon Fermi surface have an infinite number of gapless modes, but on a finite width cylinder, there are only finite numbers of them. A fitting of central charge c has been done by analyzing the entanglement entropy calculated with DMRG, which measures the number of gapless modes and is found to increase roughly linearly with the width of the cylinder, consistent with the SFS phase. As discussed in the Supplemental Material [39], the central charge can, in principle, distinguish between the U(1) and Z2 QSL. Unfortunately, in the SFS phase the entanglement entropy converges slowly when we increase the number of states in DMRG, and it is not possible to extract the central charge unambiguously. On the other hand, the positions of peaks as well as the spin structure factor converge faster, as shown in Fig 3.

Another interesting finding is the VBS phase. As shown in the phase diagram (Fig. 1), at intermediate K/J, there is a VBS phase that is revealed by the dimer-dimer correlation. We clearly observe y-direction dimer structure with a sharp peak at the M $(\frac{1}{2}\mathbf{b}_1 + \frac{1}{2}\mathbf{b}_2)$ point [39]. From the continuous dependence of energy on K/J in our DMRG simulation on finite sizes, it is very likely that the transition from AFM to VBS or VBS to SFS is a continuous one, where the AFM to VBS transition may generate a deconfined quantum critical point (DQCP) [52] and is worth further study.

As we have previously mentioned, the anisotropy in $1T$-TaS_2 is actually small. We have explored the effect of this small anisotropy to the phase diagram, and found that the small anisotropy moderately suppresses the region of the VBS phase and thus helps stabilize the QSL phase.

Discussion and conclusions.—We have derived the effective spin model for $1T$-TaS_2. It is an XXZ model with four-spin ring exchange on the triangular lattice. This effective model supports a SFS ground state with spinon Fermi surface at moderate to large K/J regions. We clearly observe the singular wave vectors in the spin structure factor from the $2k_F$ surface that can be described by a half-filled spinon with a uniform hopping on the triangular lattice.

Finally, we remark on the applicability of these results to $1T$-TaS_2. Our monolayer model is directly applicable to monolayer $1T$-TaS_2 which can be grown by MBE. For bulk samples, if the interlayer coupling is weaker than the intralayer exchange J, it is possible that the ground state is made up of weakly coupled layers of SFS. It will be of great interest to use neutron scattering to look for the $2k_F$ peaks in the static spin structure factor $S(\mathbf{k})$. Furthermore, the SFS state is expected to have low energy excitations concentrated around $2k_F$. Gapless excitations are also expected for $k < 2k_F$ and to extend to an energy scale which is a fraction of the spinon bandwidth. This is seen in calculations based on the free spinon model [53]. The SFS is expected to have finite spin susceptibility. Experimentally there is indeed a residual temperature independent susceptibility [11], but it is not known how much of it is spin or orbital in origin. We also expect a linear term γ in the specific heat. This is seen experimentally but it is suppressed by a magnetic field [13]. This contribution has been explained as mainly due to the local moment [54]. If we use the large magnetic field limit to extract an intrinsic γ, we find a value of about 0.1 $\mathrm{mJ/K^2}$ per mole of TaS_2 or 1.3 $\mathrm{mJ/K^2}$ per mole of star of David cluster. This is about a factor of 10 smaller than what is observed in the organics [2,3], suggesting that the exchange energy scale is a factor of 10 larger. This value of γ is on the small side and had prompted two of us to rule out a spinon Fermi surface in an earlier study [10]. The small value of γ may simply reflect a large exchange scale. Another intriguing option is that the Fermi surface has been partially gapped in the direction of the M point by spinon pairing, as discussed earlier in this Letter. From the experimental side, we are encouraged by a recent report of a linear T term in the thermal conductivity [55], which is usually taken as a signature of mobile gapless fermions. In an insulator the only plausible candidate is a full or partial spinon Fermi surface. While an earlier study reported a null result [12], we note that the discrepancy may be due to sample quality, since thermal conductivity depends linearly on the scattering time, and is therefore sensitive to the amount of magnetic impurities which strongly scatter the spinons.

An exciting future avenue is the doping of the weak Mott insulator. Doping of the spinon Fermi surface spin liquid

will likely lead to a correlation driven superconductor [56]. As discussed earlier [10], the interesting regime is a doping concentration of about 10% per cluster which is less than 1% per Ta. Carrier localization is a serious challenge at such a low doping level and gating of atomically thin samples may be the preferred method. The recent success of inducing superconductivity by doping the weak Mott insulator in twisted bilayer graphene is certainly encouraging [57]. The $1T$-TaS_2 system has the advantage of having a much higher temperature scale compared with graphene and the organics.

X. Y. Xu is thankful for the discussion with E. M. Stoudenmire and Donna Sheng. The calculations are performed using the ITensor C++ library (version 2.1.1). W.-Y. He, X. Y. Xu, and K. T. L. are thankful for the support of HKRGC through HKUST3/CRF/13G and C6026-16W. W.-Y. He also acknowledges the support of the Hong Kong PhD Fellowship. G. C. is supported by the Ministry of Science and Technology of China with the Grant No. 2016YFA0301001 and the Thousand-Youth-Talent Program of China. K. T. L. is further supported by the Croucher Foundation and the Dr Tai-chin Lo Foundation. P. A. L. acknowledges support by the U.S. Department of Energy, Basic Energy Sciences under Grant No. DE-FG02-03-ER46076. P. A. L. also is thankful for the hospitality of the Institute for Advanced Studies at the Hong Kong University of Science and Technology. The simulation is performed at the Tianhe-2 platform at the National Supercomputer Center in Guangzhou.

*wanderxu@gmail.com
†palee@mit.edu
‡phlaw@ust.hk

[1] P. Anderson, Mater. Res. Bull. **8**, 153 (1973).
[2] Y. Shimizu, K. Miyagawa, K. Kanoda, M. Maesato, and G. Saito, Phys. Rev. Lett. **91**, 107001 (2003).
[3] T. Itou, A. Oyamada, S. Maegawa, M. Tamura, and R. Kato, J. Phys. Condens. Matter **19**, 145247 (2007).
[4] M. P. Shores, E. A. Nytko, B. M. Bartlett, and D. G. Nocera, J. Am. Chem. Soc. **127**, 13462 (2005).
[5] Y. Okamoto, M. Nohara, H. Aruga-Katori, and H. Takagi, Phys. Rev. Lett. **99**, 137207 (2007).
[6] Y. Li, H. Liao, Z. Zhang, S. Li, F. Jin, L. Ling, L. Zhang, Y. Zou, L. Pi, Z. Yang, J. Wang, Z. Wu, and Q. Zhang, Sci. Rep. **5**, 16419 (2015).
[7] Y. Li, G. Chen, W. Tong, L. Pi, J. Liu, Z. Yang, X. Wang, and Q. Zhang, Phys. Rev. Lett. **115**, 167203 (2015).
[8] Y. Shen, Y.-D. Li, H. Wo, Y. Li, S. Shen, B. Pan, Q. Wang, H. Walker, P. Steffens, M. Boehm *et al.*, Nature (London) **540**, 559 (2016).
[9] J. A. Paddison, M. Daum, Z. Dun, G. Ehlers, Y. Liu, M. B. Stone, H. Zhou, and M. Mourigal, Nat. Phys. **13**, 117 (2017).
[10] K. T. Law and P. A. Lee, Proc. Natl. Acad. Sci. U.S.A. **114**, 6996 (2017).
[11] M. Klanjšek, A. Zorko, J. Mravlje, Z. Jagličić, P. K. Biswas, P. Prelovšek, D. Mihailovic, D. Arčon, and R. Žitko, Nat. Phys. **13**, 1130 (2017).
[12] Y. J. Yu, Y. Xu, L. P. He, M. Kratochvilova, Y. Y. Huang, J. M. Ni, L. Wang, S.-W. Cheong, J.-G. Park, and S. Y. Li, Phys. Rev. B **96**, 081111 (2017).
[13] A. Ribak, I. Silber, C. Baines, K. Chashka, Z. Salman, Y. Dagan, and A. Kanigel, Phys. Rev. B **96**, 195131 (2017).
[14] Z. Feng, Z. Li, X. Meng, W. Yi, Y. Wei, J. Zhang, Y.-C. Wang, W. Jiang, Z. Liu, S. Li, F. Liu, J. Luo, S. Li, G.-q. Zheng, Z. Y. Meng, J.-W. Mei, and Y. Shi, Chin. Phys. Lett. **34**, 077502 (2017).
[15] Z. Ding, Y. Yang, J. Zhang, C. Tan, Z. Zhu, G. Chen, and L. Shu, arXiv:1802.00968.
[16] Special issue, A. Kitaev, Ann. Phys. (Amsterdam) **303**, 2 (2003).
[17] L. Balents, Nature (London) **464**, 199 (2010).
[18] S. Yan, D. A. Huse, and S. R. White, Science **332**, 1173 (2011).
[19] S. Depenbrock, I. P. McCulloch, and U. Schollwöck, Phys. Rev. Lett. **109**, 067201 (2012).
[20] H.-C. Jiang, Z. Wang, and L. Balents, Nat. Phys. **8**, 902 (2012).
[21] H. J. Liao, Z. Y. Xie, J. Chen, Z. Y. Liu, H. D. Xie, R. Z. Huang, B. Normand, and T. Xiang, Phys. Rev. Lett. **118**, 137202 (2017).
[22] Y. Iqbal, F. Becca, S. Sorella, and D. Poilblanc, Phys. Rev. B **87**, 060405 (2013).
[23] S. J. Miyake, J. Phys. Soc. Jpn. **61**, 983 (1992).
[24] A. V. Chubukov, S. Sachdev, and T. Senthil, J. Phys. Condens. Matter **6**, 8891 (1994).
[25] S. R. White and A. L. Chernyshev, Phys. Rev. Lett. **99**, 127004 (2007).
[26] P. H. Y. Li, R. F. Bishop, and C. E. Campbell, Phys. Rev. B **91**, 014426 (2015).
[27] Z. Zhu and S. R. White, Phys. Rev. B **92**, 041105 (2015).
[28] W.-J. Hu, S.-S. Gong, W. Zhu, and D. N. Sheng, Phys. Rev. B **92**, 140403 (2015).
[29] R. Kaneko, S. Morita, and M. Imada, J. Phys. Soc. Jpn. **83**, 093707 (2014).
[30] Y. Iqbal, W.-J. Hu, R. Thomale, D. Poilblanc, and F. Becca, Phys. Rev. B **93**, 144411 (2016).
[31] There is spatial anisotropy in organic compounds κ-$(BEDT\text{-}TTF)_2Cu_2(CN)_3$ [2] and $EtMe_3Sb[Pd(dmit)_2]_2$ [3].
[32] O. I. Motrunich, Phys. Rev. B **72**, 045105 (2005).
[33] S.-S. Lee and P. A. Lee, Phys. Rev. Lett. **95**, 036403 (2005).
[34] D. N. Sheng, O. I. Motrunich, and M. P. A. Fisher, Phys. Rev. B **79**, 205112 (2009).
[35] M. S. Block, D. N. Sheng, O. I. Motrunich, and M. P. A. Fisher, Phys. Rev. Lett. **106**, 157202 (2011).
[36] P. Fazekas and E. Tosatti, Philos. Mag. B **39**, 229 (1979).
[37] K. Rossnagel and N. V. Smith, Phys. Rev. B **73**, 073106 (2006).
[38] B. Sipos, A. F. Kusmartseva, A. Akrap, H. Berger, L. Forró, and E. Tutiš, Nat. Mater. **7**, 960 (2008).
[39] See Supplemental Material at http://link.aps.org/supplemental/10.1103/PhysRevLett.121.046401 for details on the effective model, DMRG simulation, and how to determine different phases, which includes Refs [40–43].
[40] V. Heine, Phys. Rev. **153**, 673 (1967).

[41] A. H. MacDonald, S. M. Girvin, and D. Yoshioka, Phys. Rev. B **37**, 9753 (1988).
[42] L. Savary and L. Balents, Rep. Prog. Phys. **80**, 016502 (2017).
[43] P. Calabrese and J. Cardy, J. Stat. Mech. (2004) P06002.
[44] L. F. Mattheiss, Phys. Rev. B **8**, 3719 (1973).
[45] N. V. Smith, S. D. Kevan, and F. J. DiSalvo, J. Phys. C **18**, 3175 (1985).
[46] P. Darancet, A. J. Millis, and C. A. Marianetti, Phys. Rev. B **90**, 045134 (2014).
[47] S. Qiao, X. Li, N. Wang, W. Ruan, C. Ye, P. Cai, Z. Hao, H. Yao, X. Chen, J. Wu, Y. Wang, and Z. Liu, Phys. Rev. X **7**, 041054 (2017).
[48] J. Villain, R. Bidaux, J.-P. Carton, and R. Conte, J. Physique **41**, 1263 (1980).
[49] K. Kubo and T. Momoi, Z. Phys. B **103**, 485 (1997).
[50] Except the calculation with magnetic fields, which is performed with general DMRG.
[51] S.-S. Lee, P. A. Lee, and T. Senthil, Phys. Rev. Lett. **98**, 067006 (2007).
[52] T. Senthil, A. Vishwanath, L. Balents, S. Sachdev, and M. P. A. Fisher, Science **303**, 1490 (2004).
[53] Y.-D. Li, Y.-M. Lu, and G. Chen, Phys. Rev. B **96**, 054445 (2017).
[54] I. Kimchi, J. P. Sheckelton, T. M. McQueen, and P. A. Lee, arXiv:1803.00013.
[55] H. Murayama, Y. Sato, X. Xing, T. Taniguchi, S. Kasahara, Y. Kasahara, M. Yoshida, Y. Iwasa, and Y. Matsuda, arXiv:1803.06100.
[56] P. W. Anderson, Science **235**, 1196 (1987).
[57] Y. Cao, V. Fatemi, S. Fang, K. Watanabe, T. Taniguchi, E. Kaxiras, and P. Jarillo-Herrero, Nature (London) **556**, 43 (2018).